Published online 17 September 2015

Nucleic Acids Research, 2016, Vol. 44, No. 2 ***e13***
doi: 10.1093/nar/gkv893

Polysome shift assay for direct measurement of miRNA inhibition by anti-miRNA drugs

John R. Androsavich[1,*], Daniel J. Sobczynski[2], Xueqing Liu[1], Shweta Pandya[1], Vivek Kaimal[1], Tate Owen[1], Kai Liu[1], Deidre A. MacKenna[1] and B. Nelson Chau[1]

[1]Regulus Therapeutics Inc., 3545 John Hopkins Ct, San Diego, CA 92121, USA and [2]Department of Chemical Engineering, University of Michigan, Ann Arbor, MI, USA

Received July 17, 2015; Revised August 17, 2015; Accepted August 25, 2015

ABSTRACT

Anti-miRNA (anti-miR) oligonucleotide drugs are being developed to inhibit overactive miRNAs linked to disease. To help facilitate the transition from concept to clinic, new research tools are required. Here we report a novel method—miRNA Polysome Shift Assay (miPSA)—for direct measurement of miRNA engagement by anti-miR, which is more robust than conventional pharmacodynamics using downstream target gene derepression. The method takes advantage of size differences between active and inhibited miRNA complexes. Active miRNAs bind target mRNAs in high molecular weight polysome complexes, while inhibited miRNAs are sterically blocked by anti-miRs from forming this interaction. These two states can be assessed by fractionating tissue or cell lysates using differential ultracentrifugation through sucrose gradients. Accordingly, anti-miR treatment causes a specific shift of cognate miRNA from heavy to light density fractions. The magnitude of this shift is dose-responsive and maintains a linear relationship with downstream target gene derepression while providing a substantially higher dynamic window for aiding drug discovery. In contrast, we found that the commonly used 'RT-interference' approach, which assumes that inhibited miRNA is undetectable by RT-qPCR, can yield unreliable results that poorly reflect the binding stoichiometry of anti-miR to miRNA. We also demonstrate that the miPSA has additional utility in assessing anti-miR cross-reactivity with miRNAs sharing similar seed sequences.

INTRODUCTION

Numerous reports have implicated aberrant microRNA (miRNA) activity in diseases such as inflammatory disease, fibrosis and cancer. In an attempt to antagonize overactive miRNAs, chemically modified anti-miR oligonucleotides have been designed to sterically inhibit miRNAs via complementary base pairing (1–3). These anti-miRs have been shown to improve disease outcome in a number of preclinical animal studies, including an anti-miR-21 in surgically-induced kidney injury models of kidney fibrosis and genetic-engineered Alport nephropathy models (4,5), as well as an anti-miR-103 in diabetic mice (6). Importantly, two chemically unique anti-miR-122 compounds have now been shown as proof of concept in Phase I/II clinical trials to reduce Hepatitis C Virus viral titer (7,8). Collectively, these results have reinforced miRNAs' attractiveness as drug targets, and have increased enthusiasm for future anti-miR drug development.

Pharmacology studies are on the critical path toward developing anti-miR medicines. A common approach for drug-target engagement has been to assess the amount of detectable miRNA remaining after anti-miR treatment (Figure 1). High-affinity anti-miRs generally do not induce miRNA degradation but rather sequester cognate miRNA in a stable duplex (9–11). This duplex is, in theory, resistant to hybridization by reverse transcription primers, therefore measuring miRNA levels with and without anti-miR treatment is expected to provide an estimate of percent inhibition. Although this approach, referred to herein as RT-interference, has frequently been reported in literature (12–19), its accuracy has not been demonstrated and some have questioned its validity (3,9).

A more functional, yet distal, measurement of anti-miR drug activity can be made by assessing derepression of downstream miRNA regulated genes. Currently, identifying and validating miRNA targets as pharmacodynamic (PD) biomarkers is non-trivial. Although developments in computational prediction (20–23) and biochemical methods (24–26) are welcome advancements, the validation process continues to present challenges *in vivo*. Additionally, the small magnitude of target gene derepression observed (1.1–2-fold) (27), especially when combined with biological and technical variability, is often too narrow of a window for making confident drug discovery decisions such as lead compound selection and early go/no-go determina-

*To whom correspondence should be addressed. Tel: +1 858 202 6313; Fax: +1 858 202 6363; Email: johnandrosavich@gmail.com

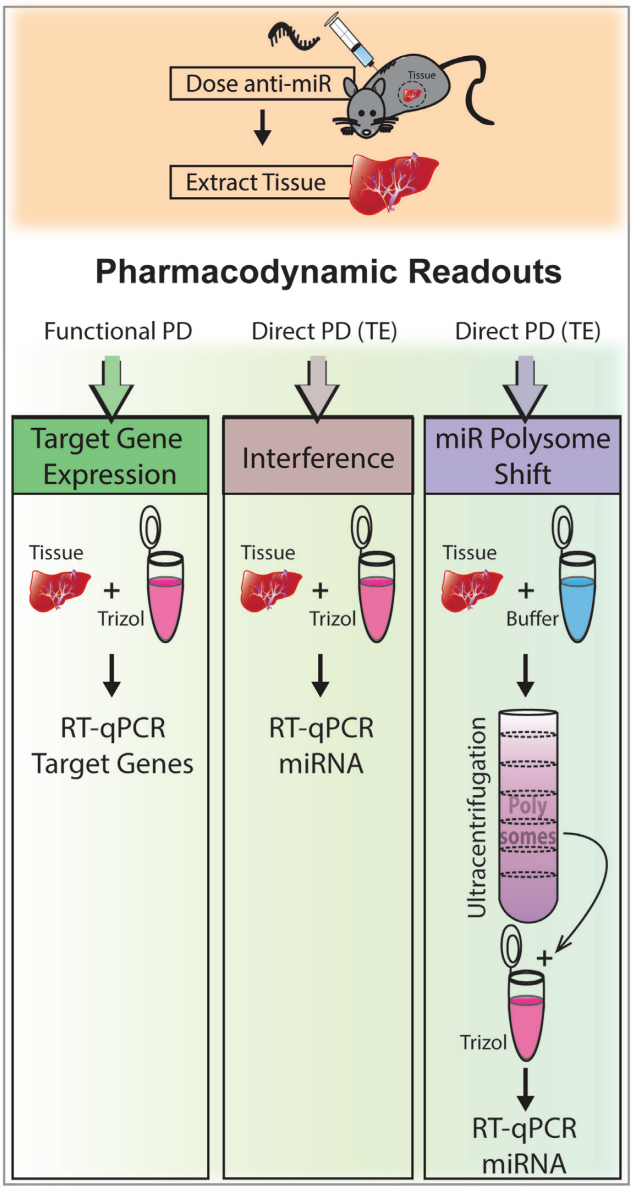

Figure 1. Schematic overview of available methods for measuring pharmacodynamics (PD) of anti-miR drugs. Following *in vivo* dosing tissue is harvested and processed for total RNA using phenol/chloroform (Trizol) and cartridge purification. RNA can be analyzed with RT-qPCR using gene specific primers to measure functional changes in miRNA regulated gene expression, or using miRNA primers to measure direct PD/drug-target engagement (TE) by RT-interference. An alternative strategy for measuring direct PD reported herein is the miRNA Polysome Shift Assay, which adds a fractionation step before RNA processing and miRNA RT-qPCR. This adds several benefits as described in the main text.

tion. Since target repression (and reciprocal derepression) is generally positively correlated with miRNA levels relative to those of target mRNAs (12,21), this problem is exacerbated in pharmacology studies using healthy animals where basal levels of miRNA targets of interest are, often by definition, low compared to disease models. Additional mechanisms may also dampen miRNA activity in the absence of stress (28,29).

Here, we report the development and validation of the miRNA Polysome Shift Assay (miPSA) as a new tool for assessing anti-miR drug binding to the site of action. miPSA serves as a complementary measure to functional PD (i.e. target gene derepression) that provides comparably greater dynamic range with defined upper and lower boundaries that are independent of target miRNA expression level. The readout is specific and requires only probes against the target and a reference miRNA. The ability to robustly and reliably measure drug-target engagement is expected to accelerate the discovery process and maximize the potential for this exciting new class of drugs.

MATERIALS AND METHODS

Animal care and treatments

All animal experiments were conducted according to the Institutional AAALAC Guidelines. Male C57BL/6 mice (Jackson Laboratories) were housed 4–5 animals per cage with a 12 h light/dark cycle. Anti-miR oligonucleotides were dissolved in 1x PBS and administered to mice by subcutaneous injection at doses and frequencies described in the results section. At time of harvest, mice were humanely sacrificed by exposure to CO_2 or isoflurane (5% v/v), and euthanasia was confirmed by cervical dislocation. Dissected tissues were weighed and flash frozen in liquid nitrogen.

Cell culture

mIMCD-3 cells (ATCC, CRL-2123) were cultured in DMEM:F12 medium supplemented with 10% fetal bovine serum in 6-well culture plates. Anti-miRs were transfected with RNAiMax (Life Technologies) as per manufacturer's protocol. In preparation for miPSA, cells were incubated with cycloheximide (100 μg/ml) added to the growth media for 15–20 min at 37°C. After, cells were washed twice with ice-cold PBS with cycloheximide. 500 μl chilled Cell Lysis Buffer (20 mM HEPES, 125 mM KCl, 5 mM $MgCl_2$, 1X HALT® Protease inhibitor, 100 μg/ml cycloheximide, 100 U/ml RNAse Out (Life Technologies), 2 mM DTT and 0.5% NP-40) was added to each well and the plate was set on ice for 10 min with occasional shaking to lyse the cells. Lysates were collected and cleared with a single bench top centrifugation step at 16 000xg for 10 min at 4°C. Supernatants were loaded on sucrose gradients and processed for miPSA as described below.

Measurement of target gene expression

Tissue samples, weighing ∼30 mg, were homogenized in Qiazol and total RNA was extracted using RNeasy® 96-well spin-plates as instructed by the manufacturer (Qiagen). RNA integrity was confirmed on an Agilent 2100 Bioanalyzer. Random cDNA was synthesized using a High Capacity cDNA Reverse Transcription kit with 50–200 ng RNA input (Life Technologies). After reverse transcription was complete, cDNA was diluted 1:3 with ddH2O and a 2.0 μl volume was used as input for each 10 μl qPCR reaction prepared with Universal TaqMan Master Mix II without UNG (Applied Biosystems) and TaqMan primer/probesets (IDT).

miRNA polysome shift assay (miPSA)

Frozen tissues, weighing 100–200 mg, were placed in Lysing Matrix D Fast-Prep Tubes (MP Biomedicals) containing 500 μl ice cold detergent-free buffer (10 mM Tris pH 7.4, 100 mM NaCl, 2.5 mM $MgCl_2$) supplemented with 100 μg/ml cycloheximide (EMD) and EDTA-free HALT® protease inhibitor cocktail (ThermoFisher). Samples were homogenized in a tissue homogenizer, shaking at 2000 oscillations/min for 60–120 s. Resulting homogenates were cleared by centrifugation at 1000xg for 10 min at 4°C. Supernatants were then centrifuged twice at 16 000xg for 10 min at 4°C. Resulting S16 lysates were layered on top of 5–60% sucrose gradients and spun in an XL-90 ultracentrifuge at 40 000 rpm for 1.5 h using a SW41 rotor (Beckman Coulter). Gradients were fractionated into 15 or 8 equal volumes by either a piston gradient fractionater (BioComp Instruments) or STAR-series liquid handling robot (Hamilton). Polysome-containing fractions were confirmed by in-line UV (254 nm) measurements or Quant-iT® RiboGreen RNA reagent (Life Technologies). Polysome-containing fractions were then analyzed using miRNA TaqMan assays (Life Technologies) to quantify relative levels of the miR-of-interest (MOI; i.e. the miRNA being inhibited) and a reference (REF) miRNA. Relative displacement of the MOI normalized to the REF was then calculated between treated and control samples using the ΔΔCT method. Displacement values are reported in $\log_2$ scale such that positive values reflect loss of miRNA from polysome fractions (i.e. displacement = ΔΔCT).

RT-interference

RT-interference was assessed using Taqman miRNA assays (Life Technology) with input of 30–100 ng total RNA extracted with RNeasy® 96-well spin plates from intact liver or kidney tissue or from S16 lysates prepared as described above. For annealing experiments, synthetic guide strand (IDT) miR-122 or miR-21 (sequences from www.mirbase.org (30)) were annealed with anti-miR in PBS using a thermal cycler with a programmed ramp down from 85°C to 10°C at a rate of 0.1°C/s. Annealed miRNA solutions were then diluted to 200 or 20 pM in a 200 μl volume containing 2 μg pre-purified total RNA isolated from kidneys of miR-21 null mice that was confirmed to contain neither miR-21 nor miR-122, the latter of which is not endogenously expressed in kidney (Figure 2C, E, F). Samples then underwent a second round of RNA purification before RT-qPCR measurements. A parallel set of reactions was prepared using 3′-Cy3 conjugated guide strands that were then run on pre-cast 20% Novex® TBE polyacrylamide gels (Life Technologies). Annealing ratios were estimated based on relative top and bottom band intensities quantified using ImageJ software (NIH).

Quantification of anti-miR

All work was carried out using high-affinity anti-miRs containing constrained ethyl (cET)-chemistries and phosphorothioate backbones. Anti-miR concentrations in sucrose gradient fractions were determined by hybridization with complementary fluorescent probes detected by high performance liquid chromatography (HPLC-FL) using an Agilent model G13321C fluorescence detector coupled to an Agilent 1260 series HPLC pump. Analysis of HPLC-FL signals was performed using MassHunter Version 7.0 (Agilent Technologies). HPLC-FL peaks were identified by comparing retention times to that of standards prepared by spiking known concentrations of anti-miR into sucrose solutions of matching density. Anti-miR concentrations in plasma samples were determined using a hybridization-based enzyme-linked immunosorbent assay (ELISA) (31). Briefly, a DNA probe containing biotin at one end and digoxigenin at the other was hybridized with analyte in plasma matrix and subsequently immobilized in a streptavidin-coated plate. Unhybridized probe was cleaved using a nuclease and then removed via a buffer wash. The digoxigenin-labeled probe was detected using anti-digoxigenin antibody conjugated to alkaline phosphatase, which catalyzed the formation of fluorescent AttoPhos® (Promega). Fluorescence intensity was determined using a fluorescence plate reader.

RESULTS

RT-interference method poorly reflects anti-miR binding

Measurement of miRNA inhibition by RT-interference is convenient and simple (Figure 1). To test the validity of the method for measuring anti-miR binding stoichiometry, we annealed synthetic miRNAs with complementary high-affinity anti-miRs in increasing ratios from sub-stoichiometric to up to 100 000-fold excess of anti-miR (Figure 2A). Annealing efficiencies were confirmed using non-denaturing PAGE (Figure 2B and D). We performed this process for two miRNA plus anti-miR combinations: one using miR-122 the other with miR-21. Annealed samples were then added back to purified total RNA depleted of endogenous miR-122 and miR-21 (see Materials and Methods). Samples then underwent a second round of trizol/cartridge RNA purification to account for any loss of miRNA:anti-miR duplex into the acidic organic phase (9).

We then evaluated whether the fraction of miRNA detectable by RT-qPCR reflected the expected annealed ratio. For miR-122, we found that RT-qPCR measurements grossly underestimated the ratio of miRNA bound to anti-miR (Figure 2B–C). Approximately 50% of miR-122 was still detectable at a 1:1 ratio (Figure 2C), where miR-122 was fully duplexed with an anti-miR-122 (Figure 2B). Only at an excess of 1000-fold did the miRNA signal begin to approach the level of background. These results suggest that RT primer can effectively compete off anti-miR for binding to miRNA. We speculate this could be related to the stem-loop structure of the RT primer (32) and/or due to enzymatic activity of the reverse transcriptase (33).

Results for miR-21 (Figure 2D–F) were even more surprising. While great excesses of anti-miR (A:M > 10 000) caused negative interference (Figure 2F), lower A:M ratios (A:M ≤ 10 000) caused an unexpected gain in signal (Figure 2E–F). This positive interference effect amplified with additional anti-miR-21 up to A:M = 10 000, which appeared to be the tipping point where the amplified signal

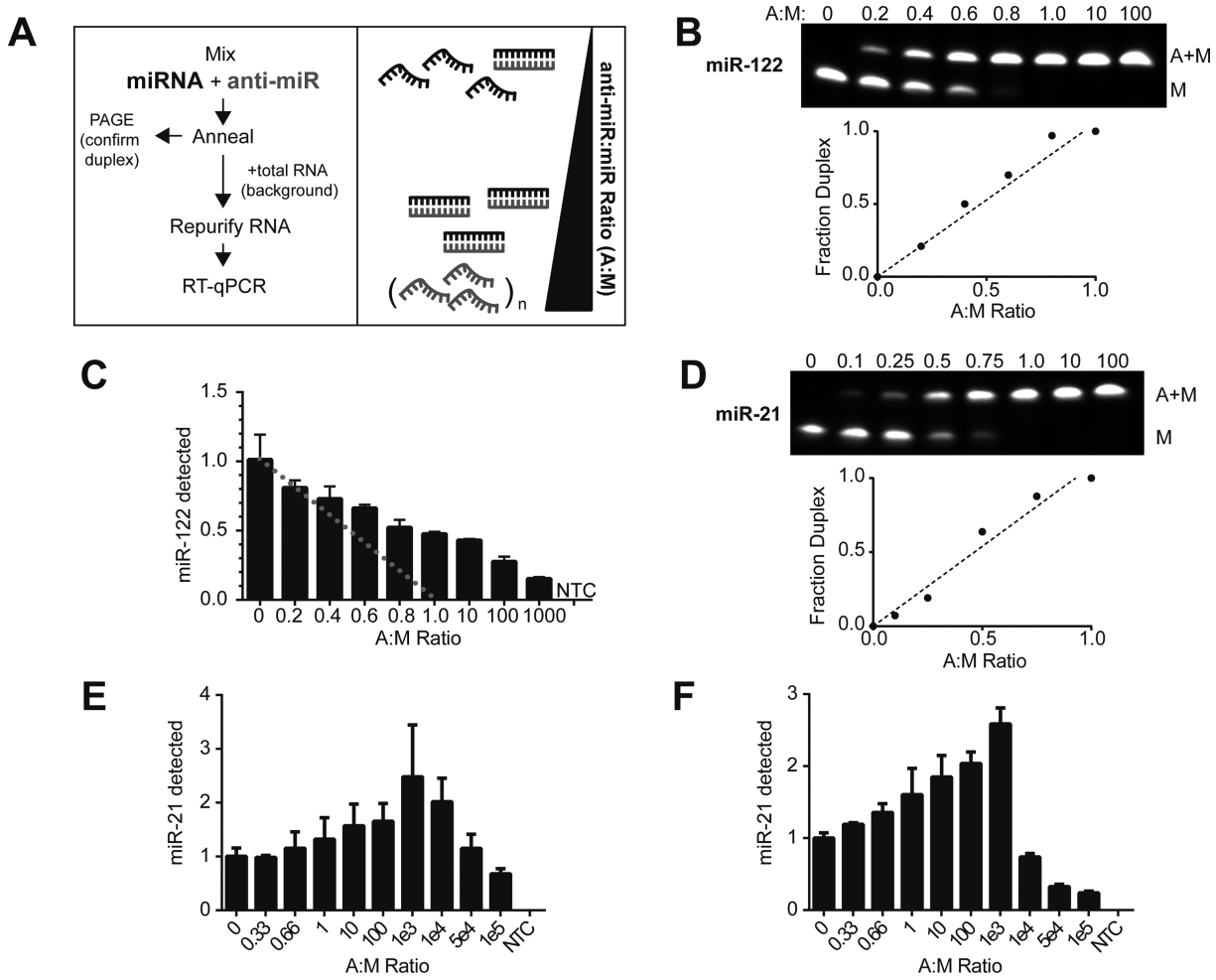

Figure 2. RT-interference poorly reflects ratios of anti-miR inhibited miRNA. (**A**) An *in vitro* annealing experiment was used to assess the ability of RT-interference to distinguish between free and anti-miR bound miRNA. Synthetic miRNA guide strand was annealed with cognate anti-miR in increasing ratios. Polyacrylamide gel electrophoresis (PAGE) was used to confirm duplex formation as ground truth for bench marking RT-interference. (**B**) Annealing efficiency of miR-122:anti-miR-122 as assessed by PAGE. A Cy3 version of miR-122 guide strand was used for detection. Duplex formation at each A:M ratio was determined by relative densitometry of lower (single-stranded) and upper (double-stranded) bands. Dashed line shows fit by least-squares linear regression ($R^2 = 0.972$). (**C**) RT-interference results using miR-122 (1e7 copies/ng RNA) and anti-miR-122 combination. Grey dashed line represents expected loss of miR-122 for each A:M ratio shown. NTC = no template control. Data are normalized to samples without anti-miR (A:M = 0). Error bars represent s.d. for n = 3 replicates. (**D**) PAGE annealing assessment of miR-21 and anti-miR-21 combination ($R^2 = 0.970$). (**E-F**) RT-interference results with (**E**) low miR-21 copy number (1e6 copies/ng RNA) and (**F**) high miR-21 (1e7 copies/ng RNA).

either decreased back toward baseline or switched to a negative effect depending on the level of miR-21 included in the sample (Figure 2E–F). While it is unclear exactly how positive interference occurs, we hypothesize that an anti-miR-21, and perhaps others, can act as a template for PCR amplification.

Regardless, these results demonstrate that, despite its convenience, the RT-interference approach in its most basic form is a poor measure of miRNA inhibition by anti-miR that can produce inaccurate and unexpected results.

miRNA polysome shift assay: validation with miR-122 in mouse liver

Our group, among others, has previously reported on the association of miRNAs and their targets in translationally active polyribosome complexes (polysomes) (34–37). This association is sensitive to translational inhibitors such as puromycin and is dependent on RNA-RNA interactions (34,35). We tested then whether disruption of miRNA-target binding in polysomes by anti-miR could be used as a quantitative readout for anti-miR activity.

miR-122 was used for the initial validation, as it represents the ideal miRNA drug target: its unique expression in hepatocytes makes it easily accessible to anti-miRs that favorably deliver to liver, and its abundance—by far the highest among miRNAs in liver—provides unusually strong repressive activity (2,38,39). As a result, several robust miR-122 target gene PD biomarkers have been validated (2,24,39), providing a good benchmark for the miPSA.

In untreated mouse liver, miR-122 was found to be well associated with polysomes (Figure 3A–B). Upon treatment with an anti-miR-122 compound, the percentage of miR-122 in polysome fractions dropped in a dose-dependent manner from ∼44% to 1.2% after 24 h (Figure 3B–C). This

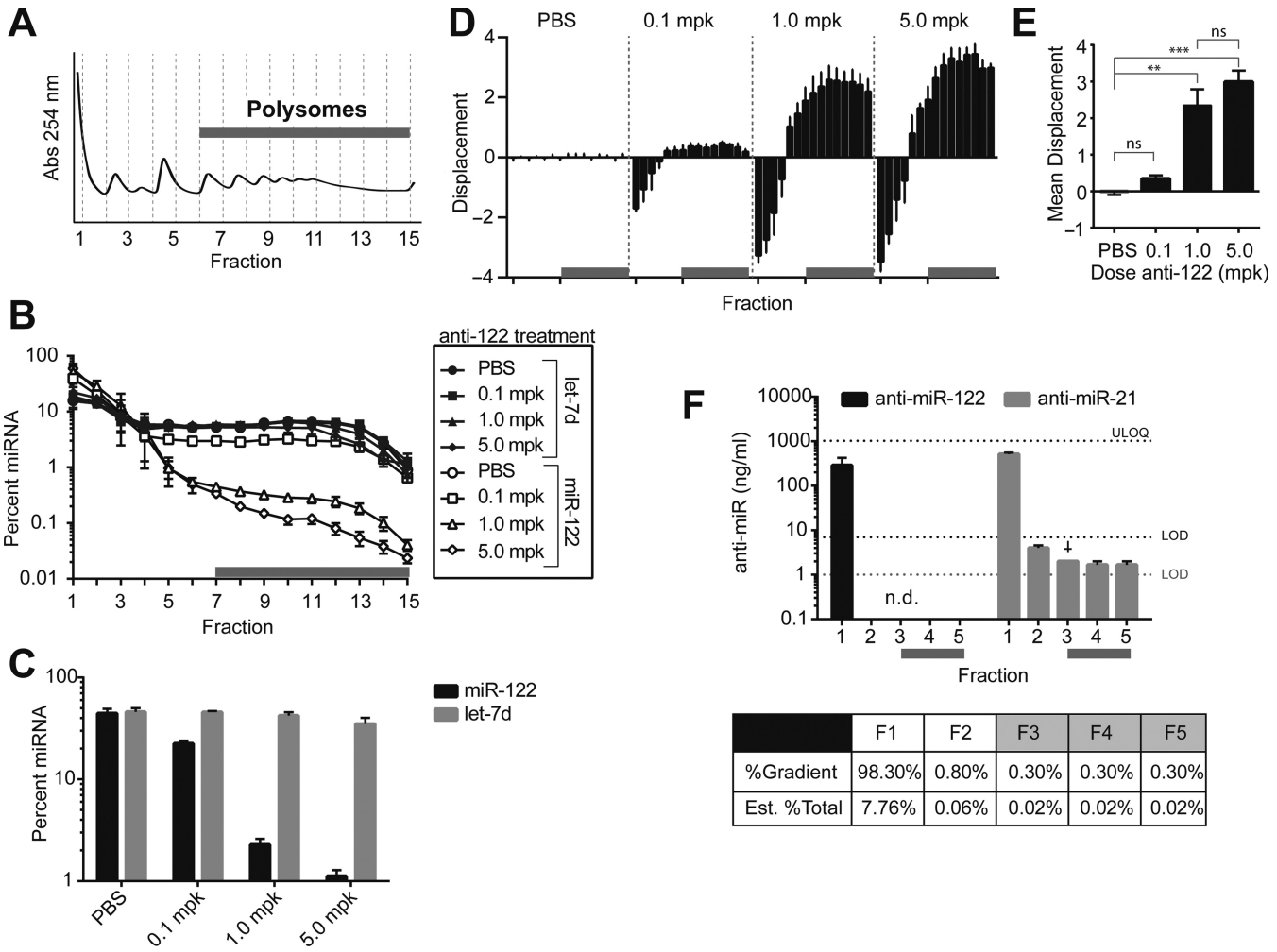

	F1	F2	F3	F4	F5
%Gradient	98.30%	0.80%	0.30%	0.30%	0.30%
Est. %Total	7.76%	0.06%	0.02%	0.02%	0.02%

Figure 3. Measurement of miR-122 inhibition by miPSA (**A**) Representative UV absorbance trace of liver lysates fractionated by ultracentrifugation through sucrose gradients. Fractions were collected from top (light) -to- bottom (dense) and are marked by their leading edge. For 15 fraction gradients, fractions 7-15 were identified as containing polysomes. In all plots, grey bar along x-axis marks polysome fractions. (**B-E**) Anti-miR-122 causes a specific dose-dependent shift of miR-122 out of polysome fractions. (**B**) RNA was isolated from each fraction and RT-qPCR was used to quantify miRNA levels. Shown are the proportions of miR-122 (open shapes) and let-7d (filled shapes) in each fraction 24 hours after treatment with anti-miR-122 or saline. For each miRNA, data were normalized to total miRNA detected across all fractions and are expressed as percent per fraction. (**C**) Cumulative percent miR-122 (black bars) or let-7d (grey bars) in polysome fractions. (**D**) The same data shown in (**B**) now showing fold-change displacement of miR-122 per fraction for each dose level of anti-miR-122 or saline. Positive displacement values are interpreted as displacement or loss of miRNA and negative values are interpreted as enrichment or gain of miRNA, relative to let-7d reference in $\log_2$ scale. (**E**) Final summary plot of average loss of miR-122 from polysome fractions for each treatment at 24 hours. ** $P < 0.01$, *** $P < 0.001$, ns = non-significant by one-way ANOVA with Tukey's post-hoc test. (**F**) (Upper graph) Quantification by HPLC-FL of anti-miR-122 (black bars) or anti-miR-21 (grey bars) in the top 5 fractions of an 8 fraction gradient. For both anti-miRs, the bulk of the oligo remained at the top of the gradient, consistent with its low molecular weight. For anti-miR-122, no anti-miR was detectable in polysome fractions above the limit of detection (LOD, marked by dotted line for each anti-miR). For anti-miR-21, trace amounts were detected in polysome fractions close to the LOD. ULOQ = upper limit of quantification. Error bars represent s.d. for n = 3 biological replicates. †One of these samples was below the LOD. (Lower table; top row) Distribution of anti-miR-21 detected in the gradient represented as percent per fraction measured. (Lower table; bottom row) Anti-miR-21 distribution in each measured fraction estimated as a percent of *total* anti-miR-21 *in tissue* based on Supplementary Figure S3.

effect was specific to miR-122 and did not occur with let-7d, a miRNA with similar basal polysome occupancy as miR-122 (Figure 3C). To improve quantification and to standardize effect size (supplementary discussion), let-7d was used as a reference and displacement scores, analogous to $\Delta\Delta$CT values obtained in the familiar $2^{-\Delta\Delta CT}$ method for relative quantification of PCR, were calculated for each fraction (Figure 3D). Closer inspection of these normalized data revealed that for miR-122 lost in polysome fractions, a reciprocal gain in miR-122 was observed in light fractions. We note, however, that recovery of miR-122 mass balance was incomplete, likely due to RT-interference effects from anti-miR-122 present in light fractions (Figure 3F). Importantly, little-to-no anti-miR was detected in polysome fractions, thus enabling artifact-free quantification in these regions of the gradient (Figure 3F). Summary statistics were then computed for each sample by taking the mean displacement across all polysome fractions (Figure 3E). Alternatively, a subset of polysome fractions could be sampled to sufficiently estimate the mean, thus decreasing processing

time. Represented this way, these data clearly showed a steep differential in shifts between 0.1 and 1.0 mg/kg body weight (mpk) dose levels, with less significant differences observed between the top doses of 1.0 and 5.0 mpk (Figure 3E).

Next, we tested the effects of anti-miR-122 as a function of time by comparing miPSA and target gene derepression at 1 and 7 days post treatment. At both time points, anti-miR induced dose-responsive derepression of miR-122 target genes *Aldoa* and *Cd320* (Figure 4A). Similar trends were observed in displacement of miR-122 from polysomes, but with a larger dynamic window than either of the genes readouts—approximately 4-fold (linear) greater maximum response at the highest dose, where both measurements approached saturation (Figure 4A). Overall displacement scores strongly correlated with target gene derepression (Figure 4C). Additionally, both readouts similarly showed greater response at the day 7 time point compared to day 1 (Figure 4A). Within 8 h after injection >99.5% of the anti-miR-122 (relative to C_{max}) was cleared from plasma and quickly taken up into hepatocytes (Figure 4B). This suggests that while anti-miR levels in liver tissue are established shortly after treatment, additional time is required for anti-miR to reach the active site (40,41). That target genes and miPSA both show this delayed PD response strongly argues against miPSA displacement being induced by post-lysis leakage of otherwise inactive anti-miR oligonucleotides.

To measure RT-interference, miRNA levels were measured using TaqMan miRNA expression assays with input from RNA extracted directly from treated tissue (Figure 1; Materials and Methods). Unlike the linear trend observed with miPSA, RT-interference exhibited a hyperbolic relationship with target gene derepression (Figure 4D): at low doses of anti-miR, RT-interference underestimated PD compared to target genes; while at high doses of anti-miR, RT-interference exaggerated PD after target gene response already saturated. These trends closely reflected those observed with annealed miRNAs *in vitro* (Figure 2C).

Taken together, these results demonstrate that miPSA, but not RT-interference, can be used as a surrogate PD measure for target gene derepression, with the advantage of having a greater dynamic window than even the most robust target genes.

Measuring anti-miR-21 pharmacology in unstressed tissue

miR-21 is an attractive drug target, especially for kidney disease where its role has been validated through genetic knockout models (4,5). Under healthy conditions, however, miR-21 seemingly rests in an inactive state with minimal target gene repression (5,34), thus making it challenging to study anti-miR-21 pharmacology by conventional means.

We treated animals with an anti-miR-21 compound and observed a dose-responsive and specific shift in miR-21 from liver polysomes (Figure 5A). Notably, the maximal shift observed at day 7 was comparable in magnitude to that of miR-122 (Figure 4A), despite that miR-122 is more highly expressed and has greater polysome occupancy (34). This finding supports that miRNA polysome shift has a common upper limit related to maximal inhibition (supplementary discussion); thus making the readout both easy to interpret and universal between different miRNAs, sample-types, and experiments.

Despite lack of a global transcriptomic signature (5,34), in healthy liver tissue we were able to identify several target genes (all containing 3′ UTR miR-21 seed-match sites) that reproducibly showed weak fold-change in response to anti-miR-21 compounds but not a control mismatched anti-miR (Supplementary Figure S1). Summing $\log_2$ fold-changes across these genes generated a composite score that was dose-responsive in liver (Figure 5A). Again, miPSA provided an enhanced dynamic window while still correlating with target gene derepression (Figure 5B). The correlation, however, was lower for miR-21 ($r = 0.787$; Figure 5B) than for miR-122 ($r = 0.9065$; Figure 4C), which may be attributed to additional noise in miR-21's less robust target genes. In agreement, higher correlation coefficients were observed using the miR-21 composite score compared to using any individual gene (Figure 5B).

In kidney with low doses of anti-miR-21 (≤3 mpk), miPSA responses were similar to liver (Figure 5C; Supplementary Figure S2). However, responses began to diverge at higher doses (>3 mpk), where kidney PD appeared to saturate at a lower maximal response (Figure 5C). This suggests that full miR-21 inhibition is more difficult to achieve in total kidney tissue than it is in liver, consistent with known limitations in the ability of certain nephron segments to productively uptake oligo (42). Perhaps for the same reason, or due to tissue-dependent activities, measurable derepression of the miR-21 target gene signature was not reliably observed in unstressed kidney (data not shown). While this prevented a direct comparison, miR-21 shift in kidney displayed similarly delayed kinetics as to what had been previously observed for target genes (Figures 4A and 5D). Therefore, miPSA is capable of measuring miRNA inhibition even where target gene response is weak due to lack of stress and/or incomplete delivery.

We again evaluated RT-interference for comparison. As described above, *in vitro* annealing experiments had shown an unexpected gain in miR-21 amplification in the presence of an anti-miR-21 (Figure 2E–F). Using intact liver tissue treated *in vivo*, this same effect was not observed (Figure 5E). Rather, RT-interference worked as one might hope: increasing dosage of anti-miR-21 negatively interfered with miR-21 detection, and loss of miR-21 signal was found to linearly correlate with target gene derepression (Figure 5F). Based on measurements of anti-miR tissue levels and miR-21 copies in liver (34,43), we estimated ∼7500-to-1 ratio of anti-miR-21 to miR-21 at the 45 mpk dose (supplementary discussion), approaching the upper limit tested in the *in vitro* annealing experiments where positive interference began to reverse (Figure 2E–F). The same *in vivo* samples were again measured for RT-interference after first being fractionated into S16 lysates. In this manner the near majority (∼50%) of miR-21 and other miRNAs were preserved while anti-miR that excessively resides in non-productive compartments (40,41) was depleted by >12-fold, reducing the estimated anti-miR:miR ratio to ∼1000 at 45 mpk dose (Supplementary Figure S3). Under these conditions, RT-interference no longer correlated with target gene derepression (Figure 5F). Moreover, at 5 and 15 mpk doses positive interference was again observed similar to *in vitro* annealed

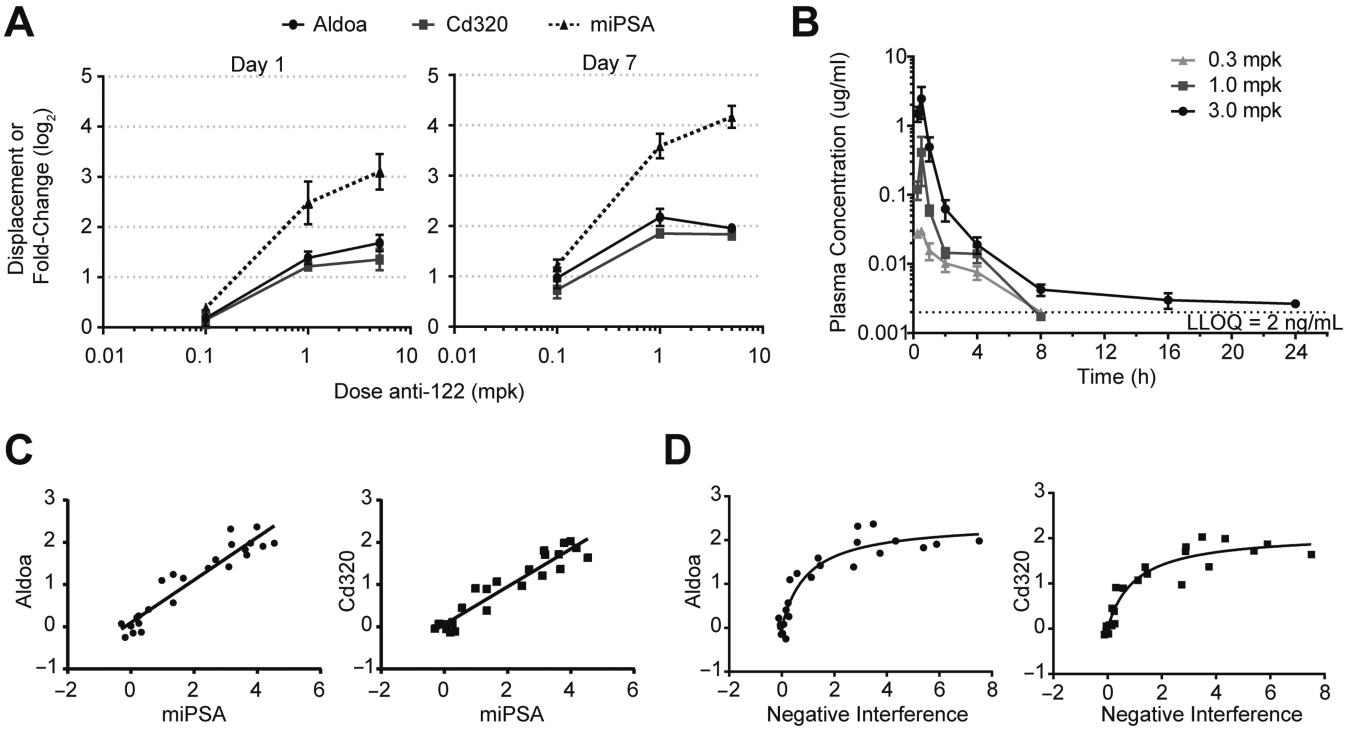

Figure 4. Comparison of miPSA with other PD methods. (**A**) Comparison of miPSA displacement (black triangle, dashed line) and mRNA expression changes of miR-122 target genes *Aldoa* (black circle, solid line) and *Cd320* (grey square, solid line) at 24 hours and 7 days post-injection of an anti-miR-122. (**B**) Time course of plasma concentrations of anti-miR-122 measured by hybridization ELISA following injection at 0.3 mpk (light grey triangle), 1.0 mpk (grey square), and 3.0 mpk (black circle). LLOQ = lower limit of quantification. (**C**) Correlation of miPSA vs *Aldoa* (left; Pearson r = 0.947, $P < 0.0001$) or *Cd320* (right; Pearson r = 0.952, $P < 0.0001$). Line represents linear regression. (**D**) Relationship between negative RT-interference and target gene derepression in $\log_2$ scale. Data shown fit with non-linear hyperbolic equation ($R^2 = 0.882$ for *Aldoa*; $R^2 = 0.907$ for *Cd320*), which fit better than linear regression ($R^2 = 0.642$ for *Aldoa*; $R^2 = 0.684$ for *Cd320*). For all plots, error bars represent s.e.m. for $n \geq 3$ replicates.

samples (Figure 5E). With increasing dosage the enhancement in signal returned to neutral at 45 mpk, suggesting that the additional anti-miR present in lysates above that of the 5 mpk dose level began to tip interference back toward a negative effect.

In all, these data indicate that under some, but not all, conditions RT-interference can indeed correlate with functional readouts of miRNA inhibition; however, this outcome is largely driven by excess non-productive anti-miR and is not truly reflective of anti-miR:miRNA stoichiometry.

Assessing intra- and inter-miRNA family cross-reactivity

Lastly, we evaluated miPSA's potential for assessing anti-miR specificity for target miRNAs with similar sequence. It is assumed that anti-miRs will cross-react with miRNA family members sharing common seed motifs, since this region of the miRNA is the determining factor for target specificity (44). This has been shown to be true for short seed-targeting anti-miRs using a luciferase reporter and pre-miRNAs co-transfected in succession (45). We tested whether miPSA could be used to directly and simultaneously measure inhibition of individual native miRNA family members.

Cultured cells were transfected with increasing doses of an anti-miR-17, and subsequently analyzed with miPSA using primers to detect miR-17 and its seed-sharing family members miR-20b and miR-106a (Figure 6A) along with additional non-related miRNAs. Consistent with intrafamily cross-reactivity, all of the miR-17 family members were strongly displaced from polysomes in a consistent dose responsive manner (Figure 6B). Non-miR-17 family miRNAs, on the other hand, were unresponsive in comparison, with one exception: miR-18a unexpectedly showed strong cross-reactivity at higher doses (Figure 6B).

Upon further inspection, we found a single nucleotide A/G difference between miR-17 and miR-18 seed sequences (Figure 6A). It has previously been shown that a single point mismatch in the seed region is sufficient to disrupt anti-miR binding (10). However, this particular nucleotide switch would form a G:U wobble pair, a common RNA:RNA interaction (46). Although the tolerability of G:U wobbles in miRNA targeting is unclear (47–49), these non-Watson Crick base pairs are frequently found to be enriched in RNAs that co-immunoprecipitate with the central miRNA factor Ago (50,51). Our data suggests that permissiveness for at least one G:U wobble pair in the seed extends to chemically modified anti-miRs as well.

DISCUSSION

Each class of nucleic acid drug has its own unique challenges for development. For anti-miRs, one of these challenges is measuring drug action. Unlike anti-sense and siRNA modalities that are designed to have a large effect

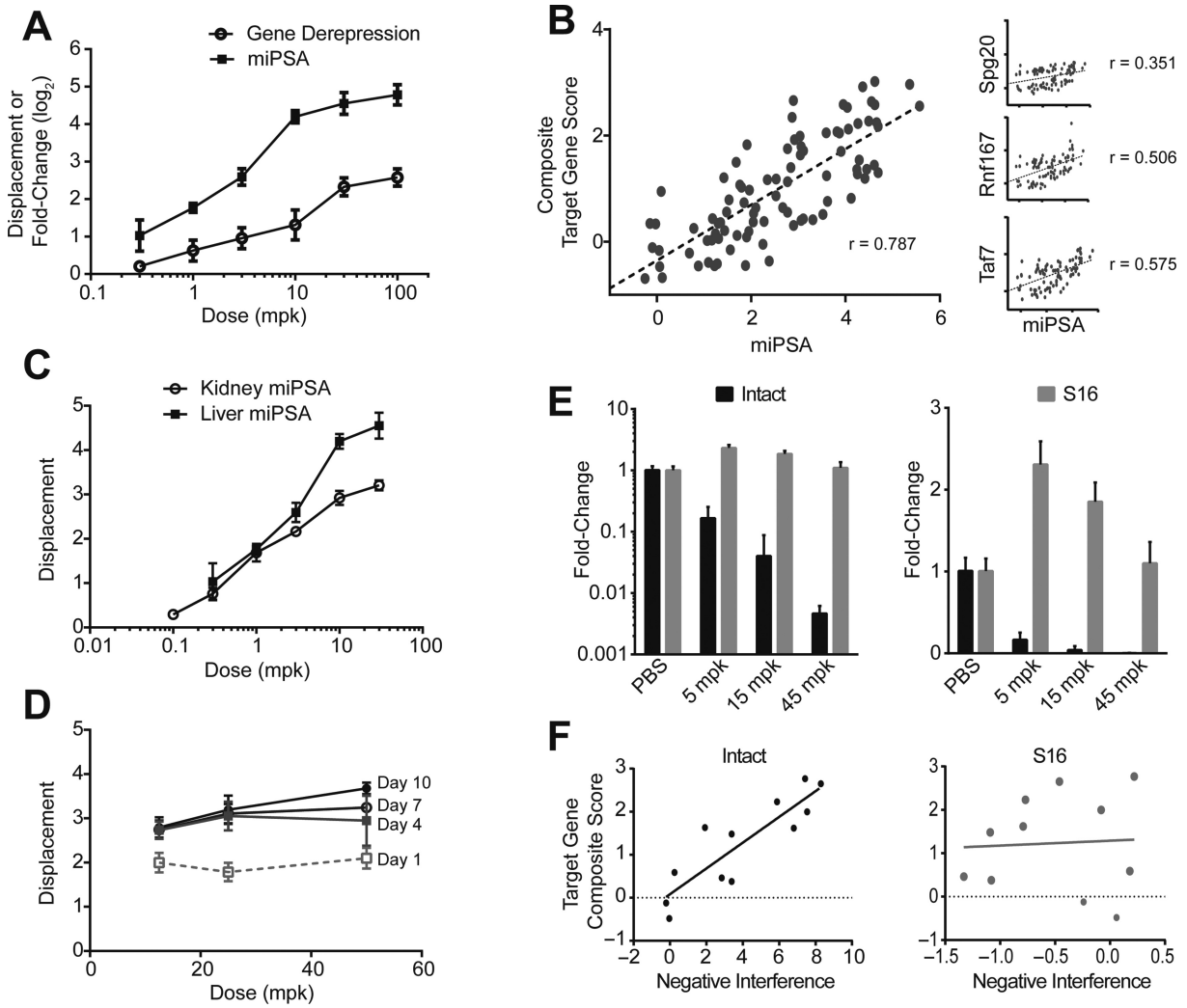

Figure 5. Measurement of miR-21 inhibition by miPSA in non-stressed tissue. (**A**) Comparison of miR-21 miPSA displacement (black squares) and target gene derepression (empty circles) in liver as a function of dose 7 days post injection. Target gene derepression represents a composite score of summed $\log_2$ fold-changes for three miR-21 seed-matched genes: *Spg20*, *Rnf167*, and *Taf7*. Error bars represent s.e.m. for n = 4 animals per group. (**B**) Correlation between miPSA and composite target gene score in liver across two independent experiments with a total n = 90 animals. Inset shows correlations for the individual miR-21 target genes. For each plot, Pearson correlation coefficients are shown with linear regression fits (dotted black lines). (**C**) Comparison of miR-21 displacement in liver (black squares) and kidney (empty circles) from the same animals. Error bars represent s.e.m. for n = 4-5 animals per group. (**D**) Time course of miR-21 displacement in kidney in dose response at day 1 (empty squares, light grey dashed line), day 4 (dark grey filled squares, solid line), day 7 (empty circles, black solid line), and day 10 (black filled circles, solid line). Error bars represent s.e.m. for n = 7 animals per group. (**E**) RT-interference measured with RNA input isolated from intact liver pieces (black bars) or S16 liver lysates (grey bars). The same data are represented on both graphs, with y-axes shown in log (left) and linear (right) scales. Data represent linear fold-changes in miR-122 normalized to let-7d and PBS samples. Error bars represent s.d. for n = 3 per group. (**F**) Correlation between target gene composite score and negative RT-interference measured from intact liver (left; black) and S16 lysates (right; grey).

on a single mRNA that is easily measured (52,53), the best readout to date for anti-miRs are downstream target genes, whose response can be both weak in magnitude and difficult to differentiate from secondary or indirect effects. Making the situation more difficult is that miRNA-mediated regulation can be context and tissue specific (5,34,51,54,55). This creates a circular problem when assessing compound delivery and activity: target genes are required to validate delivery; yet delivery is required to validate target genes.

In an effort to escape this circular logic, RT-interference has been utilized as a direct measure of miRNA inhibition (12–19). We tested the basic premise of this approach using both simple samples prepared *in vitro* with defined ratios of miRNA-to-anti-miR, as well as more complex samples using tissues from animals dosed with anti-miRs. Our results suggest that, at best, RT-interference is a qualitative measure that should be utilized with caution. Although it was able to produce relevant results in certain scenarios, we observed stark contrasts depending on the miRNA:anti-miR and the manner in which the samples were prepared. More often than not we found this readout to be unreliable.

Oddly, we observed a positive interference effect with anti-miR-21. A similar effect was previously observed in anti-miR-21 treated xenograft models (18), where a time course initially showed strong negative interference at 7 days post treatment, followed by positive interference on day 14.

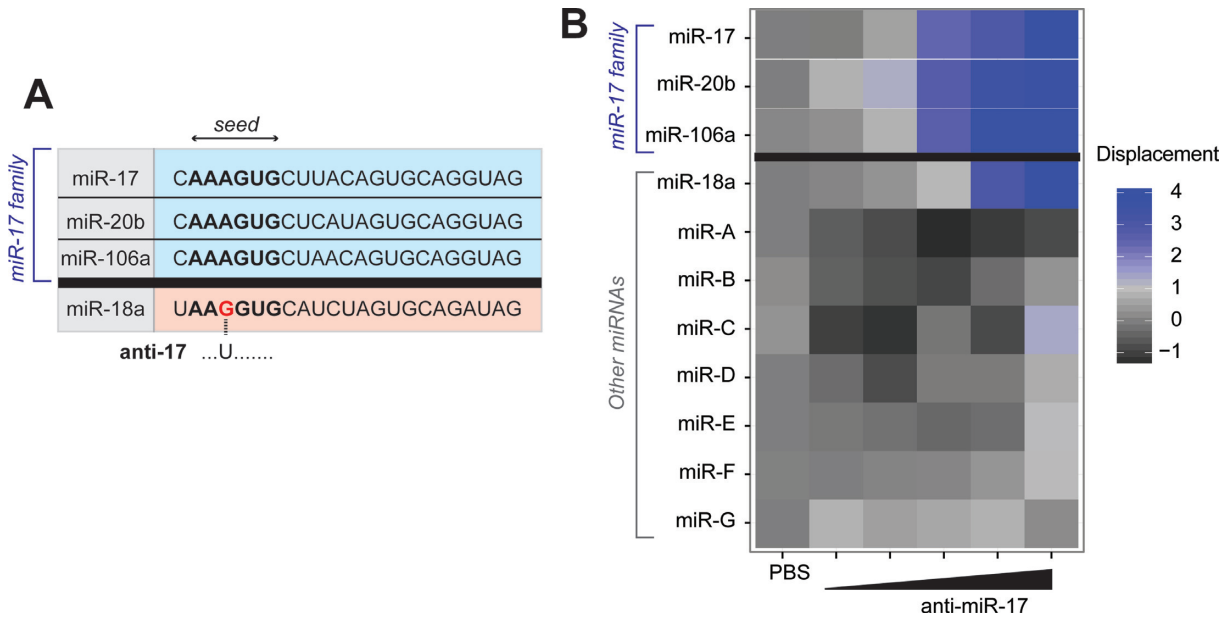

Figure 6. Assessment of anti-miR cross-reactivity using miPSA. (**A**) Alignment of mature miRNA sequences showing a common seed between miR-17 and family members miR-20b and miR-106a. Although not part of the miR-17 family, miR-18a has a near identical seed sequence apart from a single A to G change at position 4. This base could theoretically form a G:U wobble with anti-miR-17. (**B**) Heat map showing displacement of miR-17 family members and other miRNAs in response to anti-miR-17 transfected into cultured cells in dose response at 1, 3, 10, 30, and 100 nM compared to mock (PBS). Darker shades of blue represent greater mean miRNA displacement as depicted in the key.

The authors interpreted these data as anti-miR-21 having a short duration of action in the tumor; however, our data suggests that it is likely that miR-21 was still fully inhibited at day 14 but the excess anti-miR had dropped below a certain threshold. This is one example of how RT-interference data can be misleading.

As an alternative direct measure of miRNA inhibition, we developed the miPSA. Unlike RT-interference, miPSA provided consistent results across inhibition of three miRNAs in two tissues as well as cell culture. Moreover, it was especially sensitive and enabled measurement of miRNA inhibition in unstressed tissue with partial delivery, where target gene response was weak. Based on these results, we expect miPSA to be a powerful tool in breaking the delivery-target gene paradox. Once delivery and miRNA inhibition are confirmed by miPSA, target genes can be sought to understand drug mechanism of action.

Given that miRNAs are highly conserved, miPSA is likely to be translatable from mouse to non-human primates and man. This makes miPSA useful for both early and late stages of drug development, including as a potential clinical PD biomarker. In special cases interspecies cross-reactivity may not be desirable. For instance, with tumor xenograft models for oncology, it may be prudent to also measure target gene derepression using human specific primer/probe sets in order to exclude signal from mouse-derived stromal cells.

Currently, miPSA involves significant processing time, primarily due to the need for differential rate-zonal ultracentrifugation which is conventionally performed in a swinging-bucket rotor. These rotor types are currently engineered to hold only six samples per spin. We have improved processing time by simultaneously using multiple ultracentrifuges, in addition to optimizing other steps: gradient fractionation is accomplished with a robotic liquid handler and qPCR is performed in 384-well format. With the current setup, a typical *in vivo* study can be processed in 3–5 days. *In vitro*, minimum sample size is ∼2e5 cells in 6-well format. Future advancements in chromatography (56) and/or microfluidics could significantly improve the throughput and minimize the required input of this assay, thus enabling cell-type specific analysis of miRNA engagement in heterogeneous tissues like kidney.

We also demonstrated miPSA to be a useful tool for quantifying anti-miR cross-reactivity. Given the 'rules' for miRNA-mediated gene regulation (20), miRNA family members with identical seed sequences are mostly expected to have redundant repressive activities. miRNA families can also be concordantly dysregulated in disease (57,58). In these cases, high cross-reactivity of an anti-miR for all target miRNA family members is expected to have the greatest biological effect. Future studies should address more closely how varying properties of anti-miRs, such as length, affect the breadth of inhibition. In addition, we also observed cross-reactivity between anti-miR-17 and an unrelated miR-18a, likely due to a permissive G:U seed wobble. Global profiling of miRNAs in polysome fractions could uncover additional unexpected activities of anti-miRs.

In summary, given its many uses and advantages, we expect the miRNA Polysome Shift Assay to be an important addition to the researcher's toolbox for investigating the roles of miRNAs in disease and the potential therapeutic benefits of anti-miRs.

SUPPLEMENTARY DATA

Supplementary Data are available at NAR Online.

ACKNOWLEDGEMENTS

The authors thank all of their colleagues at Regulus Therapeutics for their thoughtful insights and contributions, particularly B. Bhat, A. Pavlicek, N. Gibson, J. Grundy, F. Putkey, A. Conrad and S. Neben.

FUNDING

Regulus Therapeutics, Inc., which employed all authors at the time of this work. Funding for open access charge: Regulus Therapeutics.
Conflict of interest statement. This work was funded by Regulus Therapeutics, Inc., which employed all authors.

REFERENCES

1. Meister,G., Landthaler,M., Dorsett,Y. and Tuschl,T. (2004) Sequence-specific inhibition of microRNA- and siRNA-induced RNA silencing. *RNA*, **10**, 544–550.
2. Krutzfeldt,J., Rajewsky,N., Braich,R., Rajeev,K.G., Tuschl,T., Manoharan,M. and Stoffel,M. (2005) Silencing of microRNAs in vivo with 'antagomirs'. *Nature*, **438**, 685–689.
3. Stenvang,J., Petri,A., Lindow,M., Obad,S. and Kauppinen,S. (2012) Inhibition of microRNA function by antimiR oligonucleotides. *Silence*, **3**, 1–17.
4. Gomez,I.G., MacKenna,D.A., Johnson,B.G., Kaimal,V., Roach,A.M., Ren,S., Nakagawa,N., Xin,C., Newitt,R., Pandya,S. *et al.* (2015) Anti-microRNA-21 oligonucleotides prevent Alport nephropathy progression by stimulating metabolic pathways. *J. Clin. Invest.*, **125**, 141–156.
5. Chau,B.N., Xin,C., Hartner,J., Ren,S., Castano,A.P., Linn,G., Li,J., Tran,P.T., Kaimal,V., Huang,X. *et al.* (2012) MicroRNA-21 promotes fibrosis of the kidney by silencing metabolic pathways. *Sci. Transl. Med.*, **4**, 121ra118.
6. Trajkovski,M.H., Hausser,J., Soutschek,J., Bhat,B., Akin,A., Zavolan,M., Heim,M.H. and Stoffel,M. (2011) MicroRNAs 103 and 107 regulate insulin sensitivity. *Nat. Publishing Group*, **474**, 649–653.
7. van der Ree,M.H., de Vree,J.M.L., Stelma,F., Willemse,S.B., van der Valk,M., Rietdijk,S., Molenkamp,R., Shinkel,J., Hadi,S., Harbers,M., van Vliet,A., Udo de Haes,J., Grint,P., Neben,S., Gibson,N. and Reesink,H.W. (2015) In: Levin,J (ed). *EASL - The International Liver Congress 2015*, Vienna, http://www.natap.org/2015/EASL/EASL_42.htm.
8. Janssen,H.L., Reesink,H.W., Lawitz,E.J., Zeuzem,S., Rodriguez-Torres,M., Patel,K., van der Meer,A.J., Patick,A.K., Chen,A., Zhou,Y. *et al.* (2013) Treatment of HCV infection by targeting microRNA. *New Engl. J. Med.*, **368**, 1685–1694.
9. Davis,S., Propp,S., Freier,S.M., Jones,L.E., Serra,M.J., Kinberger,G., Bhat,B., Swayze,E.E., Bennett,C.F. and Esau,C. (2009) Potent inhibition of microRNA in vivo without degradation. *Nucleic Acids Res.*, **37**, 70–77.
10. Hogan,D.J., Vincent,T.M., Fish,S., Marcusson,E.G., Bhat,B., Chau,B.N. and Zisoulis,D.G. (2014) Anti-miRs competitively inhibit microRNAs in Argonaute complexes. *PloS One*, **9**, e100951.
11. Torres,A.G., Fabani,M.M., Vigorito,E. and Gait,M.J. (2011) MicroRNA fate upon targeting with anti-miRNA oligonucleotides as revealed by an improved Northern-blot-based method for miRNA detection. *RNA*, **17**, 933–943.
12. Denzler,R., Agarwal,V., Stefano,J., Bartel,D.P. and Stoffel,M. (2014) Assessing the ceRNA hypothesis with quantitative measurements of miRNA and target abundance. *Mol. Cell*, **54**, 766–776.
13. Bertero,T., Lu,Y., Annis,S., Hale,A., Bhat,B., Saggar,R., Saggar,R., Wallace,W.D., Ross,D.J., Vargas,S.O. *et al.* (2014) Systems-level regulation of microRNA networks by miR-130/301 promotes pulmonary hypertension. *J. Clin. Invest.*, **124**, 3514–3528.
14. Montgomery,R.L., Hullinger,T.G., Semus,H.M., Dickinson,B.A., Seto,A.G., Lynch,J.M., Stack,C., Latimer,P.A., Olson,E.N. and van Rooij,E. (2011) Therapeutic Inhibition of miR-208a Improves Cardiac Function and Survival During Heart Failure. *Circulation*,**124**, 1537–1547.
15. Wurdinger,T., Tannous,B.A., Saydam,O., Skog,J., Grau,S., Soutschek,J., Weissleder,R., Breakefield,X.O. and Krichevsky,A.M. (2008) miR-296 regulates growth factor receptor overexpression in angiogenic endothelial cells. *Cancer Cell*, **14**, 382–393.
16. Brock,M., Samillan,V.J., Trenkmann,M., Schwarzwald,C., Ulrich,S., Gay,R.E., Gassmann,M., Ostergaard,L., Gay,S., Speich,R. *et al.* (2014) AntagomiR directed against miR-20a restores functional BMPR2 signalling and prevents vascular remodelling in hypoxia-induced pulmonary hypertension. *Eur. Heart J.*, **35**, 3203–3211.
17. Elmen,J., Lindow,M., Silahtaroglu,A., Bak,M., Christensen,M., Lind-Thomsen,A., Hedtjarn,M., Hansen,J.B., Hansen,H.F., Straarup,E.M. *et al.* (2008) Antagonism of microRNA-122 in mice by systemically administered LNA-antimiR leads to up-regulation of a large set of predicted target mRNAs in the liver. *Nucleic Acids Res.*, **36**, 1153–1162.
18. Frezzetti,D., De Menna,M., Zoppoli,P., Guerra,C., Ferraro,A., Bello,A.M., De Luca,P., Calabrese,C., Fusco,A., Ceccarelli,M. *et al.* (2011) Upregulation of miR-21 by Ras in vivo and its role in tumor growth. *Oncogene*, **30**, 275–286.
19. Goedeke,L., Salerno,A., Ramirez,C.M., Guo,L., Allen,R.M., Yin,X., Langley,S.R., Esau,C., Wanschel,A., Fisher,E.A. *et al.* (2014) Long-term therapeutic silencing of miR-33 increases circulating triglyceride levels and hepatic lipid accumulation in mice. *EMBO Mol. Med.*, **6**, 1133–1141.
20. Grimson,A., Farh,K.K., Johnston,W.K., Garrett-Engele,P., Lim,L.P. and Bartel,D.P. (2007) MicroRNA targeting specificity in mammals: determinants beyond seed pairing. *Mol. Cell*, **27**, 91–105.
21. Garcia,D.M., Baek,D., Shin,C., Bell,G.W., Grimson,A. and Bartel,D.P. (2011) Weak seed-pairing stability and high target-site abundance decrease the proficiency of lsy-6 and other microRNAs. *Nat. Struct. Mol. Biol.*, **18**, 1139–1146.
22. Krek,A., Grun,D., Poy,M.N., Wolf,R., Rosenberg,L., Epstein,E.J., MacMenamin,P., da Piedade,I., Gunsalus,K.C., Stoffel,M. *et al.* (2005) Combinatorial microRNA target predictions. *Nat. Genet.*, **37**, 495–500.
23. Kertesz,M., Iovino,N., Unnerstall,U., Gaul,U. and Segal,E. (2007) The role of site accessibility in microRNA target recognition. *Nat. Genet.*, **39**, 1278–1284.
24. Androsavich,J.R. and Chau,B.N. (2014) Non-inhibited miRNAs shape the cellular response to anti-miR. *Nucleic Acids Res.*, **42**, 6945–6955.
25. Beitzinger,M. and Meister,G. (2011) Experimental Identification of MicroRNA Targets by Immunoprecipitation of Argonaute Protein Complexes. *Methods Mol. Biol.*, **732**, 153–167.
26. Karginov,F.V., Conaco,C., Xuan,Z., Schmidt,B.H., Parker,J.S., Mandel,G. and Hannon,G.J. (2007) A biochemical approach to identifying microRNA targets. *Proc. Natl. Acad. Sci. U.S.A.*, **104**, 19291–19296.
27. Ebert,M.S. and Sharp,P.A. (2012) Roles for microRNAs in conferring robustness to biological processes. *Cell*, **149**, 515–524.
28. Leung,A.K. and Sharp,P.A. (2010) MicroRNA functions in stress responses. *Mol. Cell*, **40**, 205–215.
29. Mendell,J.T. and Olson,E.N. (2012) MicroRNAs in stress signaling and human disease. *Cell*, **148**, 1172–1187.
30. Griffiths-Jones,S. (2004) The microRNA Registry. *Nucleic Acids Res.*, **32**, D109–D111.
31. Yu,R.Z., Baker,B., Chappell,A., Geary,R.S., Cheung,E. and Levin,A.A. (2002) Development of an ultrasensitive noncompetitive hybridization-ligation enzyme-linked immunosorbent assay for the determination of phosphorothioate oligodeoxynucleotide in plasma. *Anal. Biochem.*, **304**, 19–25.
32. Chen,C., Ridzon,D.A., Broomer,A.J., Zhou,Z., Lee,D.H., Nguyen,J.T., Barbisin,M., Xu,N.L., Mahuvakar,V.R., Andersen,M.R. *et al.* (2005) Real-time quantification of microRNAs by stem-loop RT-PCR. *Nucleic Acids Res.*, **33**, e179.
33. Whiting,S.H. and Champoux,J.J. (1994) Strand displacement synthesis capability of Moloney murine leukemia virus reverse transcriptase. *J. Virol.*, **68**, 4747–4758.

34. Androsavich,J.R., Chau,B.N., Bhat,B., Linsley,P.S. and Walter,N.G. (2012) Disease-linked microRNA-21 exhibits drastically reduced mRNA binding and silencing activity in healthy mouse liver. *RNA*, **18**, 1510–1526.
35. Maroney,P.A., Yu,Y., Fisher,J. and Nilsen,T.W. (2006) Evidence that microRNAs are associated with translating messenger RNAs in human cells. *Nat. Struct. Mol. Biol.*, **13**, 1102–1107.
36. Nottrott,S., Simard,M.J. and Richter,J.D. (2006) Human let-7a miRNA blocks protein production on actively translating polyribosomes. *Nat. Struct. Mol. Biol.*, **13**, 1108–1114.
37. Molotski,N. and Soen,Y. (2012) Differential association of microRNAs with polysomes reflects distinct strengths of interactions with their mRNA targets. *RNA*, **18**, 1612–1623.
38. Bandiera,S., Pfeffer,S., Baumert,T.F. and Zeisel,M.B. (2015) miR-122–a key factor and therapeutic target in liver disease. *J. Hepatol.*, **62**, 448–457.
39. Esau,C., Davis,S., Murray,S.F., Yu,X.X., Pandey,S.K., Pear,M., Watts,L., Booten,S.L., Graham,M., McKay,R. *et al.* (2006) miR-122 regulation of lipid metabolism revealed by in vivo antisense targeting. *Cell Metab.*, **3**, 87–98.
40. Koller,E., Vincent,T.M., Chappell,A., De,S., Manoharan,M. and Bennett,C.F. (2011) Mechanisms of single-stranded phosphorothioate modified antisense oligonucleotide accumulation in hepatocytes. *Nucleic Acids Res.*, **39**, 4795–4807.
41. Wagenaar,T.R., Tolstykh,T., Shi,C., Jiang,L., Zhang,J., Li,Z., Yu,Q., Qu,H., Sun,F., Cao,H. *et al.* (2015) Identification of the endosomal sorting complex required for transport-I (ESCRT-I) as an important modulator of anti-miR uptake by cancer cells. *Nucleic Acids Res.*, **43**, 1204–1215.
42. Carome,M.A., Kang,Y.H., Bohen,E.M., Nicholson,D.E., Carr,F.E., Kiandoli,L.C., Brummel,S.E. and Yuan,C.M. (1997) Distribution of the cellular uptake of phosphorothioate oligodeoxynucleotides in the rat kidney in vivo. *Nephron*, **75**, 82–87.
43. Bissels,U., Wild,S., Tomiuk,S., Holste,A., Hafner,M., Tuschl,T. and Bosio,A. (2009) Absolute quantification of microRNAs by using a universal reference. *RNA*, **15**, 2375–2384.
44. Lewis,B.P., Shih,I.H., Jones-Rhoades,M.W., Bartel,D.P. and Burge,C.B. (2003) Prediction of mammalian microRNA targets. *Cell*, **115**, 787–798.
45. Obad,S., Dos Santos,C.O., Petri,A., Heidenblad,M., Broom,O., Ruse,C., Fu,C., Lindow,M., Stenvang,J., Straarup,E.M. *et al.* (2011) Silencing of microRNA families by seed-targeting tiny LNAs. *Nat. Genet.*, **43**, 371–378.
46. Varani,G. and McClain,W.H. (2000) The G x U wobble base pair. A fundamental building block of RNA structure crucial to RNA function in diverse biological systems. *EMBO Rep.*, **1**, 18–23.
47. Doench,J.G. and Sharp,P.A. (2004) Specificity of microRNA target selection in translational repression. *Genes Dev.*, **18**, 504–511.
48. Lewis,B.P., Burge,C.B. and Bartel,D.P. (2005) Conserved seed pairing, often flanked by adenosines, indicates that thousands of human genes are microRNA targets. *Cell*, **120**, 15–20.
49. Miranda,K.C., Huynh,T., Tay,Y., Ang,Y.S., Tam,W.L., Thomson,A.M., Lim,B. and Rigoutsos,I. (2006) A pattern-based method for the identification of MicroRNA binding sites and their corresponding heteroduplexes. *Cell*, **126**, 1203–1217.
50. Chi,S.W., Hannon,G.J. and Darnell,R.B. (2012) An alternative mode of microRNA target recognition. *Nat. Struct. Mol. Biol.*, **19**, 321–327.
51. Clark,P.M., Loher,P., Quann,K., Brody,J., Londin,E.R. and Rigoutsos,I. (2014) Argonaute CLIP-Seq reveals miRNA targetome diversity across tissue types. *Sci. Rep.*, **4**, 5947–5958.
52. Matsuda,S., Keiser,K., Nair,J.K., Charisse,K., Manoharan,R.M., Kretschmer,P., Peng,C.G., A,V.K.i., Kandasamy,P., Willoughby,J.L. *et al.* (2015) siRNA Conjugates Carrying Sequentially Assembled Trivalent N-Acetylgalactosamine Linked Through Nucleosides Elicit Robust Gene Silencing In Vivo in Hepatocytes. *ACS Chem. Biol.*, **10**, 1181–1187.
53. Prakash,T.P., Lima,W.F., Murray,H.M., Elbashir,S., Cantley,W., Foster,D., Jayaraman,M., Chappell,A.E., Manoharan,M., Swayze,E.E. *et al.* (2013) Lipid Nanoparticles Improve Activity of Single-Stranded siRNA and Gapmer Antisense Oligonucleotides in Animals. *ACS Chem. Biol.*, **8**, 1402–1406.
54. Nam,J.W., Rissland,O.S., Koppstein,D., Abreu-Goodger,C., Jan,C.H., Agarwal,V., Yildirim,M.A., Rodriguez,A. and Bartel,D.P. (2014) Global analyses of the effect of different cellular contexts on microRNA targeting. *Mol. Cell*, **53**, 1031–1043.
55. Bossel Ben-Moshe,N., Avraham,R., Kedmi,M., Zeisel,A., Yitzhaky,A., Yarden,Y. and Domany,E. (2012) Context-specific microRNA analysis: identification of functional microRNAs and their mRNA targets. *Nucleic Acids Res.*, **40**, 10614–10627.
56. La Rocca,G., Olejniczak,S.H., Gonzalez,A.J., Briskin,D., Vidigal,J.A., Spraggon,L., DeMatteo,R.G., Radler,M.R., Lindsten,T., Ventura,A. *et al.* (2015) In vivo, Argonaute-bound microRNAs exist predominantly in a reservoir of low molecular weight complexes not associated with mRNA. *Proc. Natl. Acad. Sci. U.S.A.*, **112**, 767–772.
57. Bertero,T., Cottrill,K., Krauszman,A., Lu,Y., Annis,S., Hale,A., Bhat,B., Waxman,A.B., Chau,B.N., Kuebler,W.M. *et al.* (2015) The microRNA-130/301 family controls vasoconstriction in pulmonary hypertension. *J. Biol. Chem.*, **290**, 2069–2085.
58. Ivanovska,I., Ball,A.S., Diaz,R.L., Magnus,J.F., Kibukawa,M., Schelter,J.M., Kobayashi,S.V., Lim,L., Burchard,J., Jackson,A.L. *et al.* (2008) MicroRNAs in the miR-106b family regulate p21/CDKN1A and promote cell cycle progression. *Mol. Cell. Biol.*, **28**, 2167–2174.